Available online at www.sciencedirect.com

ScienceDirect

Ceramics International 39 (2013) 8597–8604

CERAMICS INTERNATIONAL

www.elsevier.com/locate/ceramint

Microwave hydrothermal synthesis and photocatalytic properties of $TiO_2/BiVO_4$ composite photocatalysts

Lili Zhang, Guoqiang Tan*, Shasha Wei, Huijun Ren, Ao Xia, Yangyang Luo

Key Laboratory of Auxiliary Chemistry & Technology for Chemical Industry, Ministry of Education, Shaanxi University of Science & Technology, Xi'an 710021, China

Received 17 February 2013; received in revised form 17 March 2013; accepted 18 March 2013
Available online 17 April 2013

Abstract

$TiO_2/BiVO_4$ composite photocatalysts with heterojunction structures were synthesized by the one-step microwave hydrothermal method. The physical and photophysical properties of the as-prepared photocatalysts were fully characterized by X-ray diffraction (XRD), field emission scanning electron microscopy (FE-SEM), transmission electron microscopy (TEM), energy dispersive spectroscopy (EDS), UV–vis diffuse reflectance spectra, photoluminescence (PL) and BET surface area analysis. The photocatalytic activities were evaluated by the decolorization of rhodamine B under UV and simulated sun-light irradiation. The results reveal that the as-prepared $TiO_2/BiVO_4$ composites exhibit higher photocatalytic activities than pure $BiVO_4$. The 20% $TiO_2/BiVO_4$ sample shows the best photocatalytic activity. The enhancement of photocatalytic activity is mainly attributed to the increasing separation rate of photogenerated charge carriers. The possible photocatalytic mechanism is discussed on the basis of the calculated energy band positions.

Keywords: $TiO_2/BiVO_4$; Photocatalysis; Heterojunction; Microwave hydrothermal

1. Introduction

Semiconductor photocatalysts are widely used in hydrogen generation, solar energy utilization and environmental remediation [1–4]. Among the various semiconductor photocatalysts, TiO_2 has been applied widely because of its efficient photocatalytic activities, high physical and chemical stability, low cost and nontoxicity [5,6]. Nevertheless, due to its large band gap (E_g=3.2 eV), TiO_2 can exhibit the higher photocatalytic activity only under UV light irradiation [7]. Therefore, researchers focused on the design and development of other metal oxides capable of photoinduced charge separation upon excitation in the visible spectral region, such as $CaIn_2O_4$ [8], $InVO_4$ [9], Ag_3PO_4 [10], Bi_2WO_6 [11], Bi_2O_3 [6,12] and $BiVO_4$ [13,14]. $BiVO_4$ has attracted great attention as an inexpensive semiconductor for the splitting reaction of water into hydrogen and oxygen [15–17] and for the degradation of organic pollutants [18–21]. There are three crystal structures of $BiVO_4$: tetragonal zircon structure, monoclinic scheelite structure and tetragonal scheelite structure. Among them, monoclinic scheelite structure $BiVO_4$ (m-$BiVO_4$) with a band gap of E_g=2.40 eV exhibits the best photocatalytic performance under visible light irradiation [22,23]. However, the rapid recombination rate of electron–hole pairs is always the main drawback of m-$BiVO_4$ for application. To solve this problem, loading noble metal [24,25], loading transition metal oxides [26] and coupling other semiconductors [27] are often used as the effective modification methods. As the formation of heterojunction can significantly reduce the recombination and speed up the separation rate of photogenerated charge carriers [28], a lot of $BiVO_4$-based composites have been synthesized. Long et al. fabricated $Co_3O_4/BiVO_4$ composite photocatalyst with a p–n heterojunction semiconductor structure by the impregnation method. They showed that $Co_3O_4/BiVO_4$ composite photocatalyst presented much higher photoactivity than pure $BiVO_4$ in the degradation of phenol under visible light irradiation [29]. Su et al. reported that the macroporous V_2O_5–$BiVO_4$ composites were prepared under the assistance of colloidal carbon spheres and exhibited the enhanced photocatalytic performance [30]. Jiang et al. also prepared $V_2O_5/BiVO_4$ composite photocatalysts using

*Corresponding author. Tel.: +86 13759878391; fax: +86 029 86168688.
E-mail address: tan3114@163.com (G. Tan).

0272-8842/$ - see front matter © 2013 Elsevier Ltd and Techna Group S.r.l. All rights reserved.
http://dx.doi.org/10.1016/j.ceramint.2013.03.106

the one-step solution combustion synthesis method [31]. They investigated the photocatalytic degradation of methylene blue (MB) in the UV–vis light region and attributed the enhancement of photocatalytic activities to the separation of electron–hole pairs. However, the photocatalytic properties of coupled TiO_2/$BiVO_4$ have not been investigated extensively.

In the typical synthesis process of composite photocatalysts, the based metal oxide would be prepared first and then it would be coupled with another metal oxide by the ion impregnation method [29,32], the photodeposition method [33], the hydrothermal method [5,34] or other thermal treatments [35]. So the fabrication process of composite photocatalysts usually involves two or three steps which is very complicated. Therefore, it is very essential to find a facile and time-saving coupling method to simplify the synthesis process of composite photocatalysts.

In this study, pure $BiVO_4$ and TiO_2/$BiVO_4$ composite photocatalysts were synthesized through the one-step microwave hydrothermal method. The photocatalytic activities were evaluated by the photodegradation of rhodamine B (RhB) under UV and simulated sun-light irradiation and the possible mechanism of the enhanced photocatalytic activities of TiO_2/$BiVO_4$ composite photocatalysts was also discussed.

2. Experimental

2.1. Preparation of catalysts

All the reagents were of analytical grade and were used without any further purification. 5 mmol $Bi(NO_3)_3 \cdot 5H_2O$ was dissolved in 20 mL HNO_3 solution (4 mol/L), while 5 mmol NH_4VO_3 was dissolved in 20 mL NaOH solution (2 mol/L). After stirred separately for 30 min, the two solutions were mixed together in a molar ratio of 1:1. After the mixed solution was stirred for 20 min, a salmon pink suspension was obtained. Different amounts of $(NH_4)_2TiF_6$ were added to the suspension individually and continually stirred for 30 min to get the precursors. The obtained samples were marked with pure $BiVO_4$, 20% TiO_2/$BiVO_4$, 50% TiO_2/$BiVO_4$ and 80% TiO_2/$BiVO_4$, corresponding to the samples with molar ratios of n_{Ti}: n_{Bi} as 0%, 20%, 50% and 80%, respectively. After stirred for another 30 min, the obtained precursors were transferred into a 100 mL Teflon-lined stainless steel autoclave. The autoclave was sealed and the microwave hydrothermal reaction was carried out in it at 200 °C for 60 min. Finally, the yellow precipitates were washed with distilled water and absolute ethanol three times and then dried at 70 °C for 10 h.

2.2. Characterization of the photocatalyst

The crystalline phase of the as-prepared samples was identified by an X-ray diffractometer (XRD, D/max-2200, Rigaku, Japan) with Cu Kα radiation ($\lambda = 0.15418$ nm) in the 2θ ranging from 15° to 70°. The morphology and the particle size were examined by field emission scanning electron microscopy (FE-SEM, JSM-6700F, JEOL, Japan). The microstructures were investigated by transmission electron microscopy (TEM) and high resolution transmission electron microscopy (HRTEM, JEM-2100, Japan). The Brunauer–Emmett–Teller (BET) surface area was determined by nitrogen adsorption at 77 K on a 3H-2000 BET-M surface area analyzer. The chemical composition was determined by energy dispersive spectroscopy (EDS, JED-2200 Series, Japan). UV–vis diffuse reflectance spectra were obtained on a UV–vis spectrophotometer (Hitachi U-3900H, Japan), using $BaSO_4$ as reference. The photoluminescence (PL) spectra were recorded with a fluorescence spectrophotometer (Hitachi F-4500, Japan).

2.3. Photocatalytic properties

Photocatalytic activities were determined by the decolorization of rhodamine B (RhB) aqueous solution under UV and simulated sun-light irradiation in a quartz photochemical reactor. A 350 W xenon lamp was used as a simulated sunlight source and a 300 W mercury lamp was used as a UV light source. In the experiment, 0.1 g $BiVO_4$ was added to 50 mL RhB solution (2×10^{-5} mol/L). Before irradiation, the solution was stirred for 30 min in dark in order to reach the adsorption–desorption equilibrium. At given time intervals, 5 mL of the suspension was taken out and centrifuged to remove the photocatalyst particles. The concentration of RhB solution was determined by measuring the absorbance at 553 nm with a UV–vis spectrophotometer.

3. Results and discussion

3.1. XRD analysis

Fig. 1 shows XRD patterns of TiO_2/$BiVO_4$ samples and pure $BiVO_4$. From Fig. 1a, it can be seen that the main diffraction peaks of TiO_2/$BiVO_4$ samples are similar to those of pure $BiVO_4$ and they can be well-indexed to monoclinic $BiVO_4$ according to the JCPDS Card (no. 14-0688). However, a careful comparison shows a small peak at $2\theta = 25.4°$ in XRD patterns of TiO_2/$BiVO_4$ samples, but not in XRD patterns of pure $BiVO_4$ sample. This small peak is ascribed to the characteristic peak (101) of anatase TiO_2 (JCPDS 21–1272), indicating the existence of TiO_2. It is also found that TiO_2/$BiVO_4$ samples display higher crystallinity than the pure $BiVO_4$ sample, indicating that the addition of $(NH_4)_2TiF_6$ can enhance the crystallinity to some extent. Moreover, both the intensity ratio of (200)/(002) exactly matching with the corresponding standard value, and the obvious peak splitting of (011) at $2\theta = 18.67°$ (seen in Fig. 1b) indicate that the 20% TiO_2/$BiVO_4$ sample displays the higher crystallinity than others.

3.2. Morphology measurement

The morphology of the as-prepared samples was characterized by FE-SEM. As shown in Fig. 2a, the pure monoclinic $BiVO_4$ crystallite is spherical shape with the diameter of 1.5–3 μm which is composed of numerous $BiVO_4$ sub-nanoparticles (200–300 nm). From Fig. 2b, it can be seen that the morphology of 20% TiO_2/$BiVO_4$ is slab with the size of

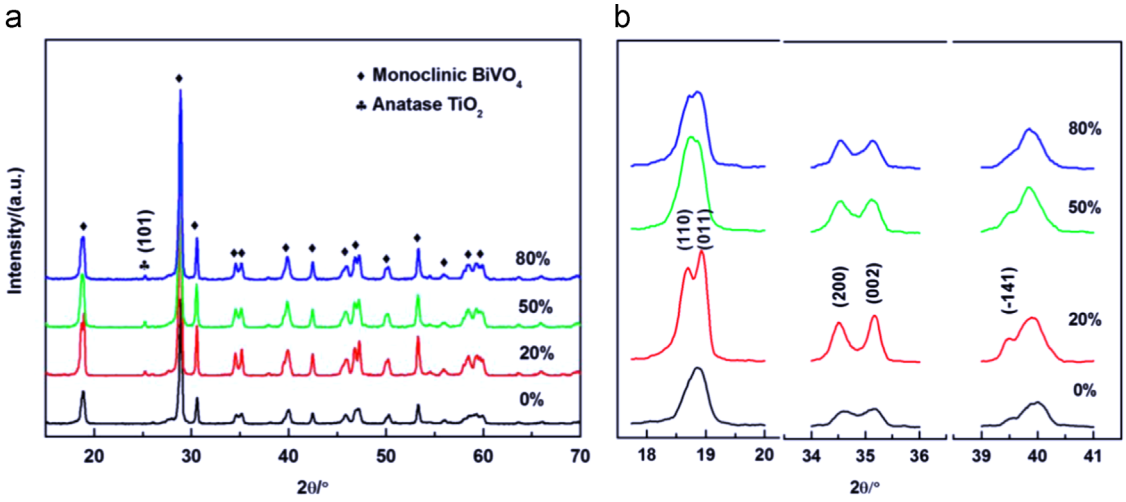

Fig. 1. XRD patterns of pure $BiVO_4$ and $TiO_2/BiVO_4$ with different TiO_2-coupled contents.

0.5–1 μm. With the increase of the TiO_2-coupled contents, the morphology of $TiO_2/BiVO_4$ is changed from slab to sphere. The uniform microspheres with the diameters of 3–4 μm or 6–7 μm are clearly observed in Fig. 2c and d.

To reveal the microstructure and the morphology of 20% $TiO_2/BiVO_4$ sample, the TEM test is carried out and the results are shown in Fig. 3. From the low magnification TEM image (Fig. 3a), it can be seen that the ultrasonic process of the preparation for TEM measurements did not cause the small TiO_2 nanoparticles to fall off $BiVO_4$ particles, indicating that TiO_2 nanoparticles have successfully grown on the surface of $BiVO_4$ particles. The high-resolution transmission electron microscopy (HRTEM) was used to further study the fine structures of nanoparticles. The HRTEM image obtained from the (b) area marked with rectangles is shown in Fig. 3b. The uniform fringes with an interval of 0.352 nm are in good agreement with the (101) lattice plane of anatase TiO_2. On the other hand, the interplanar distance of 0.236 nm agrees well with the lattice spacing at the (220) plane of the monoclinic $BiVO_4$ (shown in Fig. 3c). Thus, the results confirm that the heterojunction structure is formed from TiO_2 and $BiVO_4$.

3.3. EDS analysis

The chemical composition of each sample was determined by the EDS technique. Fig. 4 shows the average EDS signals obtained from measuring a large scale (100 times of the whole SEM image area). Besides the obvious signals of O, Bi and V elements marked in Fig. 4a, the EDS spectra show that a very weak signal of titanium with an increasing trend is detected in $TiO_2/BiVO_4$ composites. The doping contents of titanium are 7.09 at%, 7.42 at% and 7.82 at%, which are obtained from the EDS analysis. The results show that TiO_2 has been deposited on the surface of $BiVO_4$ successfully.

3.4. UV–vis diffuse absorption spectra

The energy band structure feature of a semiconductor is considered as a key factor in determining its photocatalytic activity [36]. Fig. 5 shows the UV–vis diffuse reflectance absorption spectra of the as-prepared samples. All of the samples show the strong absorption in the UV and visible-light regions. The steep shape of the spectrum indicates that the visible light absorption is not due to the transition from the impurity level but due to the band gap transition [37]. For a crystalline semiconductor, the optical absorption near the band edge follows the equation $\alpha h\upsilon = A(h\upsilon - E_g)^{n/2}$, where α, υ, E_g and A are an absorption coefficient, a light frequency, the band gap, and a constant, respectively [38]. In this work, the band gaps are estimated to be 2.17 eV, 2.04 eV, 2.17 eV and 2.16 eV from the absorption edge (inset of Fig. 5), corresponding to the pure $BiVO_4$, 20% $TiO_2/BiVO_4$, 50% $TiO_2/BiVO_4$ and 80% $TiO_2/BiVO_4$ samples, respectively. Compared with the sphere morphology, the samples with slab morphology possess the much lower band gap energy (2.04 eV), which may be ascribed to the size effect and crystal defects. The results indicate that the visible-light-response of 20% $TiO_2/BiVO_4$ composite photocatalyst is greatly improved by coupling the appropriate amount of TiO_2. Therefore, 20% $TiO_2/BiVO_4$ composite photocatalyst exhibits the higher photocatalytic efficiency than others.

3.5. Photocatalytic activities

The photocatalytic activities of the as-prepared samples were assessed by the photocatalytic degradation of RhB solutions under UV-light and simulated sun-light irradiations. Fig. 6a shows the photocatalytic activities of the photocatalysts with different concentrations of TiO_2 under UV light irradiation. It can be seen that the degradation rates of $TiO_2/BiVO_4$ samples are higher than pure $BiVO_4$. The degradation rate of 20% $TiO_2/BiVO_4$ sample is over 94% after 330 min UV irradiation, which is the best activity. Furthermore, 20% $TiO_2/BiVO_4$ sample also presents the better photocatalytic activity under simulated sun-light irradiation (Fig. 6b). All these prove that the existence of TiO_2 is much favorable to enhance the photocatalytic activities of the samples.

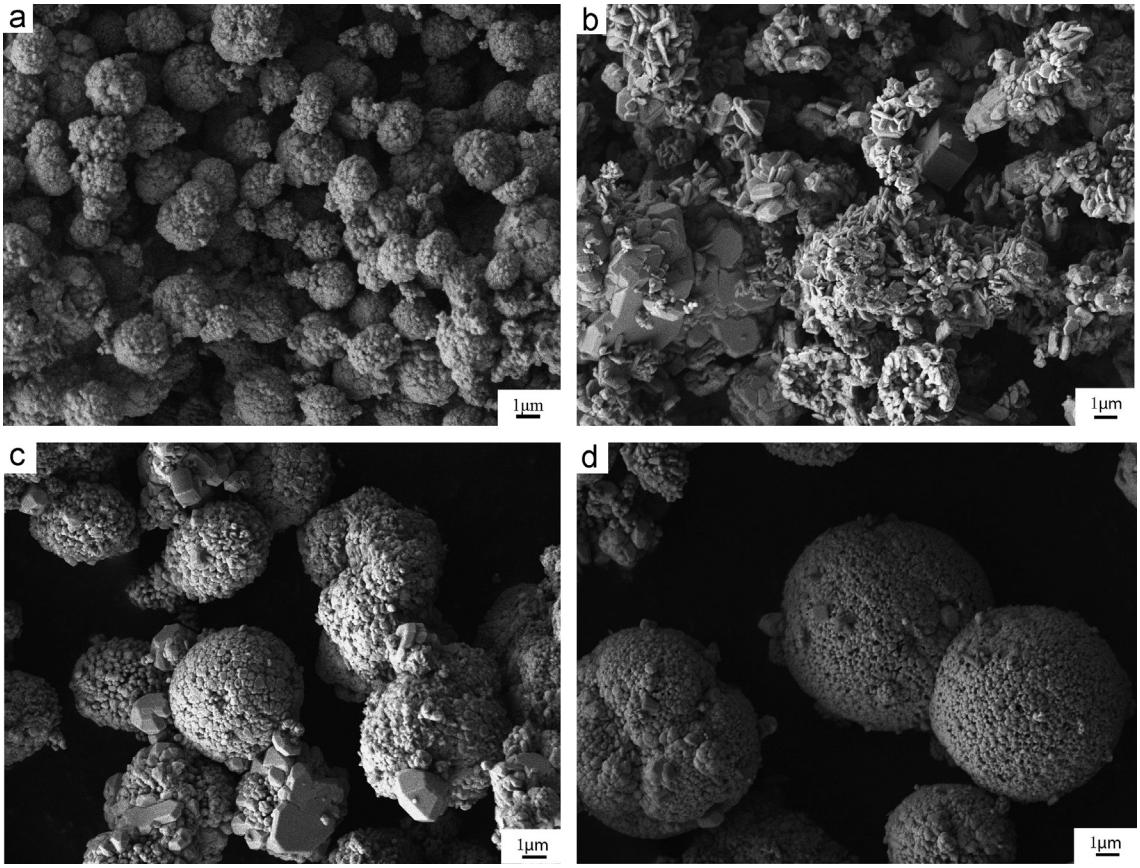

Fig. 2. FE-SEM images of (a) pure $BiVO_4$; (b) 20% $TiO_2/BiVO_4$; (c) 50% $TiO_2/BiVO_4$ and (d) 80% $TiO_2/BiVO_4$.

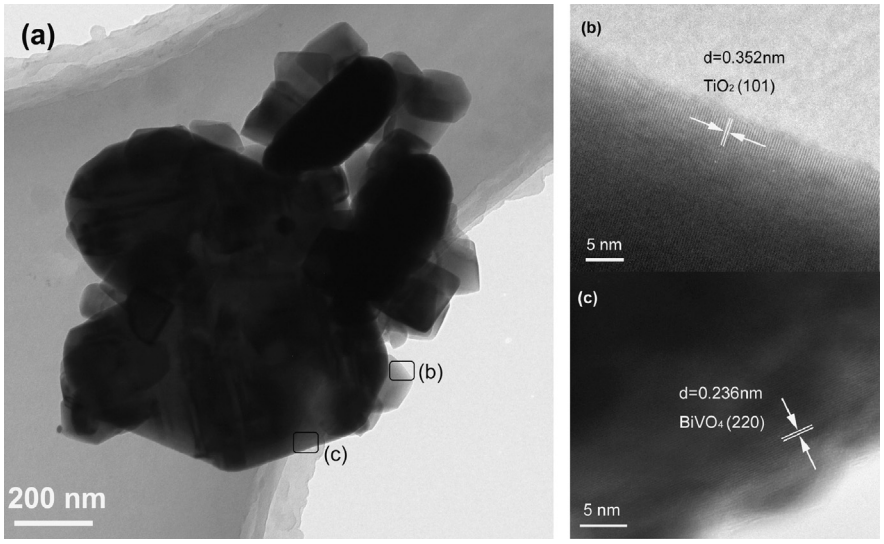

Fig. 3. (a) TEM; and (b) and (c) HRTEM images of 20% $TiO_2/BiVO_4$ sample (HRTEM images correspond to the parts marked in (a)).

3.6. Photocatalytic mechanism

The photocatalytic activity of a photocatalyst depends on various factors, including the crystal structure, crystallinity, morphology, specific surface area, light energy utilization ratio, quantum efficiency, etc., [39,40]. The larger the surface areas of the materials, the higher the photocatalytic activities they show [35]. On the basis of N_2 adsorption–desorption isotherms, the BET surface areas of pure $BiVO_4$, 20% $TiO_2/BiVO_4$, 50% $TiO_2/BiVO_4$ and 80% $TiO_2/BiVO_4$ are 0.61, 0.92, 0.91 and 0.70 m^2/g, respectively (Fig. 7). The small differences of the surface areas suggest that the surface area is not a decisive factor for the photocatalytic activities.

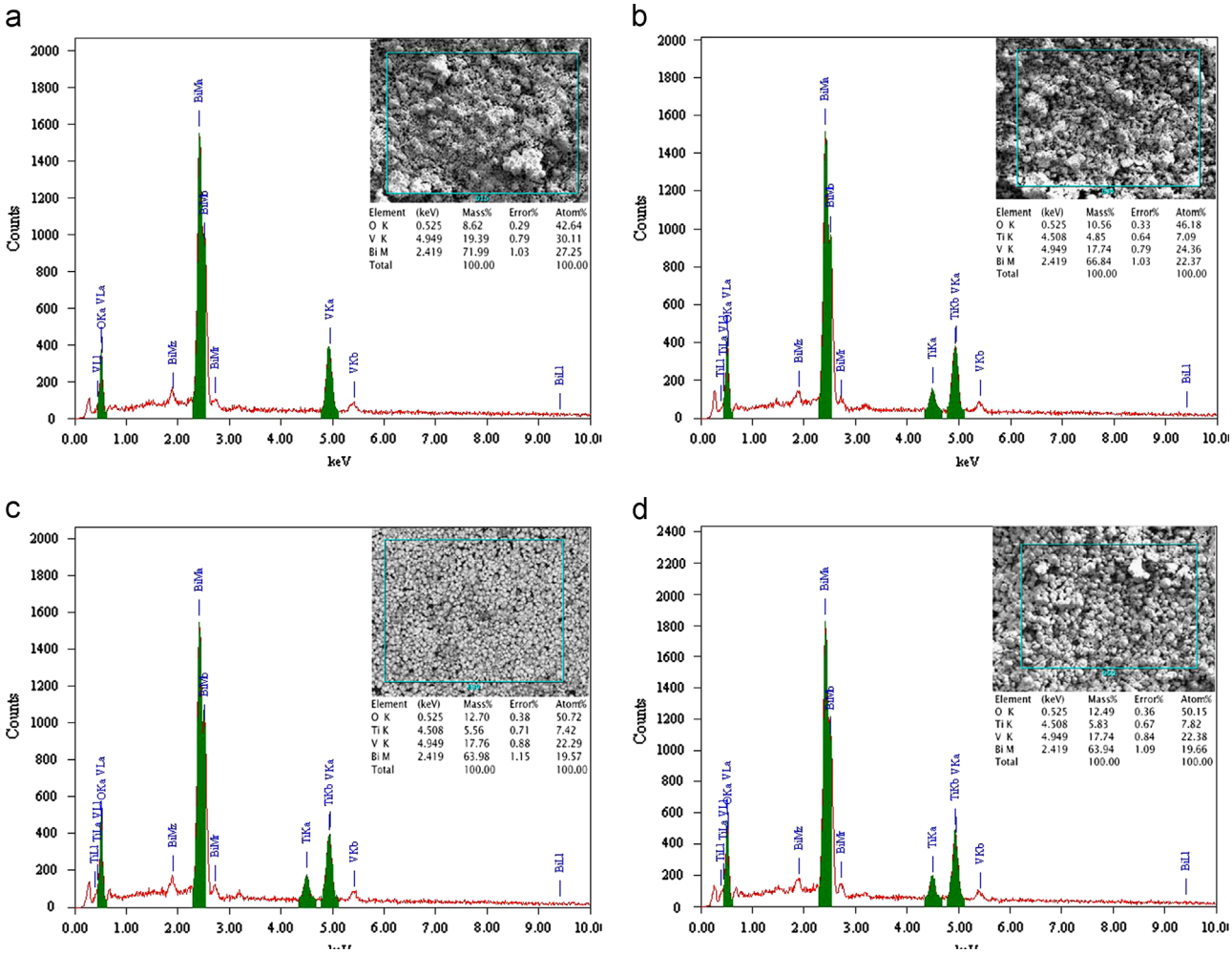

Fig. 4. EDS spectra of (a) pure $BiVO_4$; (b) 20% $TiO_2/BiVO_4$; (c) 50% $TiO_2/BiVO_4$; and (d) 80% $TiO_2/BiVO_4$.

The conduction band (CB) and valence band (VB) potentials of $BiVO_4$ and TiO_2 at the point of zero charge can be calculated by the following empirical equation [30,41]:

$$E_{VB} = \chi - E^e + 0.5E_g \quad (1)$$

where E_{VB} is the VB edge potential; χ is the electronegativity of the semiconductor, which is the geometric mean of the electronegativity of the constituent atoms (χ values of $BiVO_4$ and TiO_2 are ca. 6.04 eV [29,35] and 5.90 eV [41], respectively); E^e is the energy of free electrons on the hydrogen scale (~4.5 eV); and E_g is the band gap energy of the semiconductor. The band gap energies of $BiVO_4$ and TiO_2 are adopted as 2.17 eV and 3.20 eV [5], respectively. E_{CB} values can be obtained by $E_{CB}=E_{VB}-E_g$. The positions of the conduction and the valence bands of monoclinic $BiVO_4$ crystallites and TiO_2 crystallites calculated by Eq. (1) are listed in Table 1.

As an n-type semiconductor, TiO_2 crystallite exhibits wider band gap energy compared with $BiVO_4$ crystallites with narrow band gap energy. Thus, at the interface between TiO_2 crystallites and $BiVO_4$ crystallites, an n–n-type heterojunction structure will be formed. According to the data listed in Table 1, Scheme 1 is proposed to illustrate a possible charge-separation process [32]. As shown in Scheme 1a, under

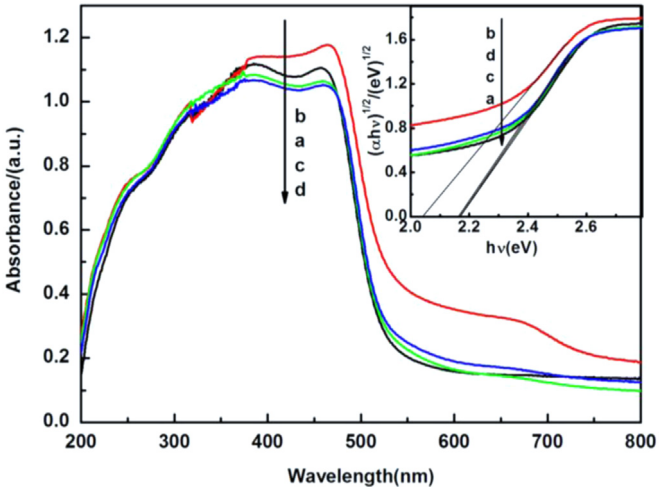

Fig. 5. UV–vis spectra of (a) pure $BiVO_4$; (b) 20% $TiO_2/BiVO_4$; (c) 50% $TiO_2/BiVO_4$; and (d) 80% $TiO_2/BiVO_4$ (inset shows the relationship between $(\alpha h\upsilon)^2$ and $(h\upsilon)$).

UV light irradiation, a dye molecule is excited to produce a singlet or triplet state (dye*). Charge is then injected into the conduction band of TiO_2 from the singlet or triplet excited

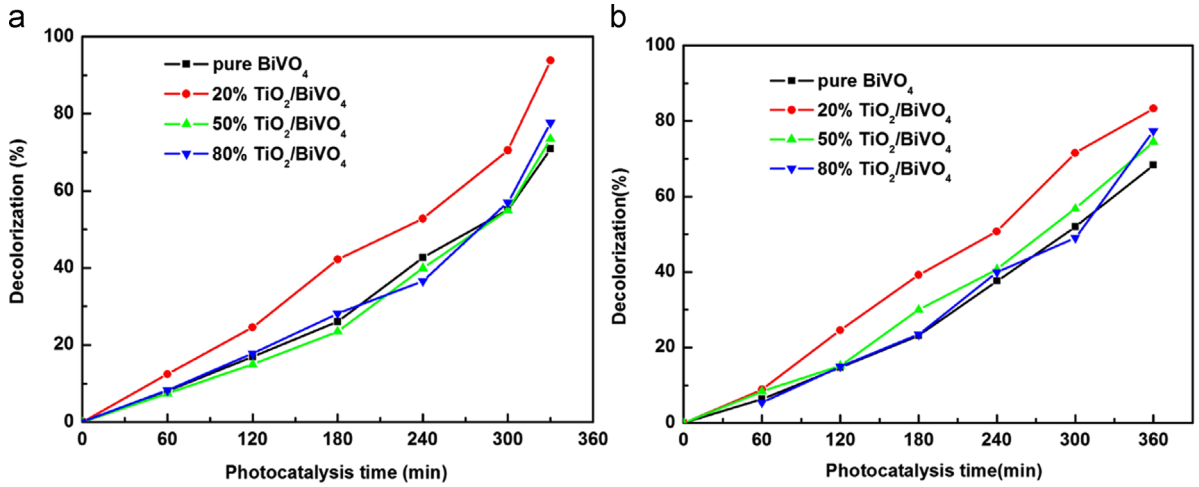

Fig. 6. RhB photocatalytic degradation curve of pure $BiVO_4$ and $TiO_2/BiVO_4$ with various TiO_2-coupled contents under UV-light irradiation (a) and simulated sun-light irradiation (b).

state of the dye [42]. Simultaneously, both $BiVO_4$ and TiO_2 could be excited by UV light so as to induce the generation of electron–hole pairs. Because the conduction band edge potential of TiO_2 (−0.20 eV) is more negative than that of $BiVO_4$ (0.46 eV), the injected electrons and photoinduced electrons on the conduction band of TiO_2 will be easily transferred to conduction band of $BiVO_4$ so as to leave holes on TiO_2 valence band. Thus the photoinduced electrons and holes are effectively separated and they can be used for degradation of RhB solutions. And there are more electrons on the surface of $BiVO_4$ to participate in the reduction reaction. Therefore, $TiO_2/BiVO_4$ samples show the higher photocatalytic activities than pure $BiVO_4$.

As shown in Scheme 1b, under simulated sun-light irradiation, the dye molecule can absorb the visible light to generate the dye* and the injected electron further moves to the conduction band of TiO_2. The injected electrons and photoinduced electrons easily flow into conduction band of $BiVO_4$ [32]. They can reduce surface chemisorbed O_2 to yield strong oxidizing radicals (such as $O_2^{\bullet -}$, $HO_2^{\bullet}$ and $OH^{\bullet}$), which can degrade the organic pollutants [42]. Because only a small amount of electrons on the valence band of TiO_2 can be excited to its conduction band under simulated sun-light irradiation, the photocatalytic efficiencies of $TiO_2/BiVO_4$ are lower than that under UV light irradiation.

In order to further confirm the above analyses, the photoluminescence (PL) test of the photocatalysts was employed to reveal the migration, the transference, and recombination processes of the photogenerated electron–hole pairs in the semiconductor [29,43]. Fig. 8 shows PL spectra of $TiO_2/BiVO_4$ samples with excitation wavelength of 290 nm. It is found that PL intensity of the 20% $TiO_2/BiVO_4$ sample is lower than other $TiO_2/BiVO_4$ samples. It is known that the weaker PL intensity is, the higher the separation efficiency of photoinduced charge is, and the higher photocatalytic activity becomes [26]. Therefore, the result indicates that compared with 50% $TiO_2/BiVO_4$ and 80% $TiO_2/BiVO_4$ samples, 20% $TiO_2/BiVO_4$ sample can be used as a higher efficient photocatalyst.

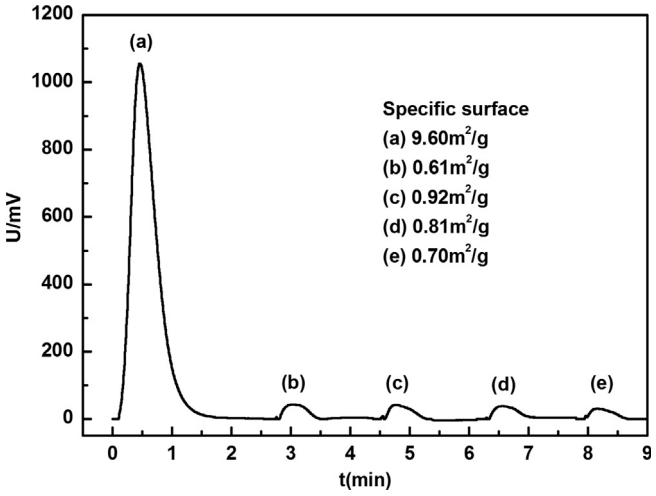

Fig. 7. Desorption curve of (a) standard sample; (b) pure $BiVO_4$; (c) 20% $TiO_2/BiVO_4$; (d) 50% $TiO_2/BiVO_4$; and (e) 80% $TiO_2/BiVO_4$.

4. Conclusions

In summary, $TiO_2/BiVO_4$ heterostructure photocatalysts have been successfully synthesized by the one-step microwave hydrothermal method. XRD patterns reveal that the as-prepared composites are composed of monoclinic $BiVO_4$ and anatase TiO_2. The anatase TiO_2 is dispersed on the surface of $BiVO_4$, which is confirmed by the EDS analysis. The results of photocatalytic activities indicate that $TiO_2/BiVO_4$ composite photocatalysts exhibit enhanced photocatalytic properties for the degradation of RhB under UV light and simulated sun-light irradiation. It is also found that the 20% $TiO_2/BiVO_4$ shows the best photocatalytic activity because of its high crystallinity, narrow band gap, and most importantly, the hierarchical heterostructure which can effectively separate photoinduced electron–hole pairs on the surface of $TiO_2/BiVO_4$ photocatalysts.

Table 1
Absolute electronegativity, energy band gap, calculated conduction band edge position and valence band edge position at the point of zero charge of TiO_2 and $BiVO_4$ semiconductors.

Semiconductors	Absolute electronegativity, χ (eV)	Calculated conduction band position (eV)	Calculated valence band position (eV)	Energy band gap, E_g (eV)
TiO_2	5.90	−0.20	3.00	3.20
$BiVO_4$	6.04	0.46	2.63	2.17

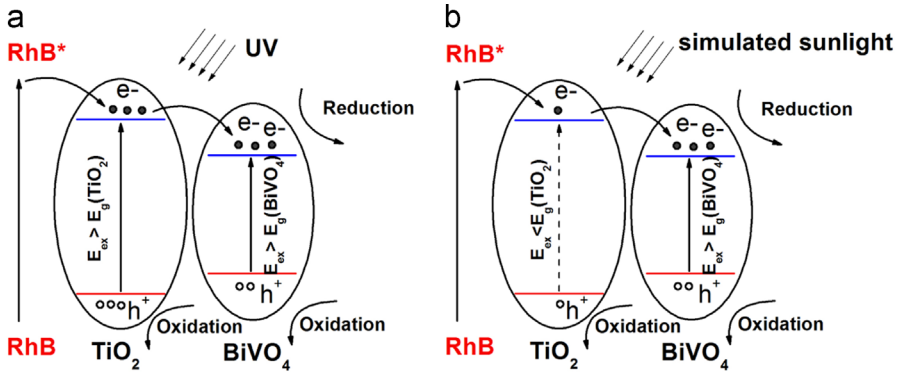

Scheme 1. Charge transfer processes of $TiO_2/BiVO_4$ heterostructure photocatalysts under UV-light irradiation (a) and simulated sun-light irradiation (b) .

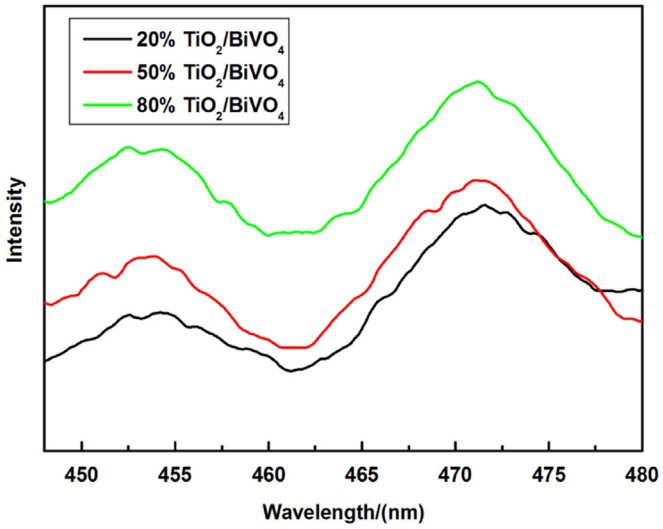

Fig. 8. PL spectra of (a) 20% $TiO_2/BiVO_4$; (b) 50% $TiO_2/BiVO_4$; and (c) 80% $TiO_2/BiVO_4$.

Acknowledgments

This work is supported by the Project of the National Natural Science Foundation of China (Grant no. 51172135); the State-Level College Students' Innovation and Entrepreneurship Training Program for Local Colleges and Universities (201210708022); the Graduate Innovation Fund of Shaanxi University of Science and Technology (SUST-A04); and the Green Manufacturing of Ceramic Materials with Novel Functional Application Innovation Team Assistance Fund of Shaanxi University of Science and Technology (TD12-05).

References

[1] Z.G. Xiong, X.S. Zhao, Nitrogen-doped titanate-anatase core–shell nanobelts with exposed {101} anatase facets and enhanced visible light photocatalytic activity, Journal of the American Chemical Society 134 (2012) 5754–5757.
[2] A. Kudo, K. Omori, H. Kato, A novel aqueous process for preparation of crystal form-controlled and highly crystalline $BiVO_4$ powder from layered vanadates at room temperature and its photocatalytic and photophysical properties, Journal of the American Chemical Society 121 (1999) 11459–11467.
[3] S.M. Sun, W.Z. Wang, L. Zhou, H.L. Xu, Efficient methylene blue removal over hydrothermally synthesized starlike $BiVO_4$, Industrial and Engineering Chemistry Research 48 (2009) 1735–1739.
[4] M.Y. Zhang, C.L. Shao, P. Zhang, C.Y. Su, X. Zhang, P.P. Liang, Y.Y. Sun, Y.C. Liu, Bi_2MoO_6 microtubes: controlled fabrication by using electrospun polyacrylonitrile microfibers as template and their enhanced visible light photocatalytic activity, Journal of Hazardous Materials 225–226 (2012) 155–163.
[5] Y. Liu, J.F. Ma, Z.S. Liu, C.H. Dai, Z.W. Song, Y. Sun, J.R. Fang, J.G. Zhao, Low-temperature synthesis of $BiVO_4$ crystallites in molten salt medium and their UV–vis absorption, Ceramics International 36 (2010) 2073–2077.
[6] S.Y. Chai, Y.J. Kim, M.H. Jung, A.K. Chakraborty, D. Jung, W.I. Lee, Heterojunctioned $BiOCl/Bi_2O_3$, a new visible light photocatalyst, Journal of Catalysis 262 (2009) 144–149.
[7] L. Zhou, W.W. Wang, S.W. Liu, L.S. Zhang, H.L Xu, W. Zhu, A sonochemical route to visible-light-driven high-activity $BiVO_4$ photocatalyst, Journal of Molecular Catalysis A: Chemical 252 (2006) 120–124.
[8] J.J. Ding, S. Sun, J. Bao, Z.L. Luo, C. Gao, Synthesis of $CaIn_2O_4$ rods and its photocatalytic performance under visible-light irradiation, Catalysis Letters 130 (2009) 147–153.
[9] Z.H. Ai, L.Z. Zhang, S.C. Lee, Efficient visible light photocatalytic oxidation of NO on aerosol flow-synthesized nanocrystalline $InVO_4$ hollow microspheres, Journal of Physical Chemistry C 114 (2010) 18594–18600.
[10] X.T. Hong, X.H. Wu, Q.Y. Zhang, M.F. Xiao, G.L. Yang, M.R. Qiu, G.C. Han, Hydroxyapatite supported Ag_3PO_4 nanoparticles with higher visible light photocatalytic activity, Applied Surface Science 258 (2012) 4801–4805.

[11] D.Q. He, L.L. Wang, H.Y. Li, T.Y. Yan, D.J. Wang, T.F. Xie, Self-assembled 3D hierarchical clew-like Bi_2WO_6 microspheres: synthesis, photo-induced charges transfer properties, and photocatalytic activities, CrystEngComm 13 (2011) 4053–4059.
[12] T. Saison, N. Chemin, C. Chaneac, O. Durupthy, V. Ruaux, L. Mariey, F. Mauge, P. Beaunier, J.P. Jolivet, Bi_2O_3, $BiVO_4$, and Bi_2WO_6: impact of surface properties on photocatalytic activity under visible light, Journal of Physical Chemistry C 114 (115) (2011) 5657–5666.
[13] Y.H. Ng, A. Iwase, A. Kudo, R. Amal, Reducing graphene oxide on a visible-light $BiVO_4$ photocatalyst for an enhanced photoelectrochemical water splitting, Journal of Physical Chemistry Letters 1 (2010) 2607–2612.
[14] M.C. Long, W.M. Cai, H. Kisch, Visible light induced photoelectrochemical properties of n-$BiVO_4$ and n-$BiVO_4$/p-Co_3O_4, Journal of Physical Chemistry C 112 (2007) 548–554.
[15] J.A. Seabold, K.S. Choi, Efficient and stable photo-oxidation of water by a bismuth vanadate photoanode coupled with an iron oxyhydroxide oxygen evolution catalyst, Journal of the American Chemical Society 134 (2012) 2186–2192.
[16] A. Kudo, Development of photocatalyst materials for water splitting, International Journal of Hydrogen Energy 31 (2006) 197–202.
[17] A. Kudo, R. Niishiro, A. Iwase, H. Kato, Effects of doping of metal cations on morphology, activity, and visible light response of photocatalysts, Chemical Physics 339 (2007) 104–110.
[18] D. Zhou, L.X. Pang, J. Guo, H. Wang, X. Yao, C. Randall, Phase evolution, phase transition, Raman spectra, infrared spectra, and microwave dielectric properties of low temperature firing $(K_{0.5x}Bi_{1-0.5x})(Mo_xV_{1-x})O_4$ ceramics with scheelite related structure, Inorganic Chemistry 50 (2011) 12733–12738.
[19] D.K. Zhong, S. Choi, D.R. Gamelin, Near-complete suppression of surface recombination in solar photoelectrolysis by Co–Pi catalyst-modified W:$BiVO_4$, Journal of the American Chemical Society 133 (2011) 18370–18377.
[20] W. Liu, Y.Q. Yu, L.X. Cao, G. Su, X.Y. Liu, L. Zhang, Y.G. Wang, Synthesis of monoclinic structured $BiVO_4$ spindly microtubes in deep eutectic solvent and their application for dye degradation, Journal of Hazardous Materials 181 (2010) 1102–1108.
[21] A.P. Zhang, J.Z. Zhang, N.Y. Cui, X.Y. Tie, Y.W. An, L.J. Li, Effects of pH on hydrothermal synthesis and characterization of visible-light-driven $BiVO_4$ photocatalyst, Journal of Molecular Catalysis A: Chemical 304 (2009) 28–32.
[22] G. Li, D. Zhang, J.C. Yu, Ordered mesoporous $BiVO_4$ through nanocasting: a superior visible light-driven photocatalyst, Chemistry of Materials 20 (2008) 3983–3992.
[23] S.W. Cao, Z. Yin, J. Barber, F.Y.C. Boey, S.C.J. Loo, C. Xue, Preparation of Au–$BiVO_4$ heterogeneous nanostructures as highly efficient visible-light photocatalysts, ACS Applied Materials and Interfaces 4 (2011) 418–423.
[24] L. Ge, Novel visible-light-driven Pt/$BiVO_4$ photocatalyst for efficient degradation of methyl orange, Journal of Molecular Catalysis A: Chemical 282 (2008) 62–66.
[25] A.P. Zhang, Z.J. Zhang, Synthesis and characterization of Ag/$BiVO_4$composite photocatalyst, Applied Surface Science 256 (2010) 3224–3227.
[26] H. Xu, H.M. Li, C.D. Wu, J.Y. Chu, Y.S. Yan, H.M. Shu, Preparation, characterization and photocatalytic activity of transition metal-loaded $BiVO_4$, Materials Science and Engineering: B 147 (2008) 52–56.
[27] L. Li, B. Yan, $BiVO_4$/Bi_2O_3 submicrometer sphere composite: microstructure and photocatalytic activity under visible-light irradiation, Journal of Alloys and Compounds 476 (2009) 624–628.
[28] L. Chen, S.F. Yin, S.L. Luo, R. Huang, Q. Zhang, T. Hong, P.C.T. Au, $Bi_2O_2CO_3$/BiOI photocatalysts with heterojunctions highly efficient for visible-light treatment of dye-containing wastewater, Industrial and Engineering Chemistry Research 51 (2012) 6760–6768.
[29] M.C. Long, W.M. Cai, J. Cai, B.X. Zhou, X.Y. Chai, Y.H. Wu, Efficient photocatalytic degradation of phenol over Co_3O_4/$BiVO_4$ composite under visible light irradiation, Journal of Physical Chemistry B 110 (2006) 20211–20216.
[30] J. Su, X.X. Zou, G.D. Li, X. Wei, C. Yan, Y.N. Wang, J. Zhao, L.J. Zhou, J.S. Chen, Macroporous V_2O_5–$BiVO_4$ composites: effect of heterojunction on the behavior of photogenerated charges, Journal of Physical Chemistry C 115 (2011) 8064–8071.
[31] H. Jiang, M. Nagai, K. Kobayashi, Enhanced photocatalytic activity for degradation of methylene blue over V_2O_5/$BiVO_4$ composite, Journal of Alloys and Compounds 479 (2009) 821–827.
[32] Y.L. Min, K. Zhang, Y.C. Chen, Y.G. Zhang, Synthesis of novel visible light responding vanadate/TiO_2 heterostructure photocatalysts for application of organic pollutants, Chemical Engineering Journal 175 (2011) 76–83.
[33] J. Wang, X.M. Fan, D.Z. Wu, J. Dai, H. Liu, H.R. Liu, Z.W. Zhou, Fabrication of CuO/T–ZnOw nanocomposites using photo-deposition and their photocatalytic property, Applied Surface Science 258 (2011) 1797–1805.
[34] N. Wetchakun, S. Chaiwichain, B. Inceesungvorn, K. Pingmuang, S. Phanichphant, A.I. Minett, J. Chen, $BiVO_4$/CeO_2 nanocomposites with high visible-light-induced photocatalytic activity, ACS Applied Materials and Interfaces 4 (2012) 3718–3723.
[35] M.L. Guan, D.K. Ma, S.W. Hu, Y.J. Chen, S.M. Huang, from hollow olive-shaped $BiVO_4$ to n–p core–shell $BiVO_4$@Bi_2O_3 microspheres: controlled synthesis and enhanced visible-light- responsive photocatalytic properties, Inorganic Chemistry 50 (2010) 800–805.
[36] M. Shang, W.W. Wang, L. Zhou, S.M. Sun, W.Z. Yin, Nanosized $BiVO_4$ with high visible-light-induced photocatalytic activity: ultrasonic-assisted synthesis and protective effect of surfactant, Journal of Hazardous Materials 172 (2009) 338–344.
[37] L. Zhou, W. Wang, L. Zhang, H.L. Xu, W. Zhu, Single-crystalline $BiVO_4$ microtubes with square cross-sections: microstructure, growth mechanism, and photocatalytic property, Journal of Physical Chemistry C 111 (2007) 13659–13664.
[38] B. Pare, B. Sarwan, S. Jonnalagadda, Photocatalytic mineralization study of malachite green on the surface of Mn-doped BiOCl activated by visible light under ambient condition, Applied Surface Science 258 (2011) 247–253.
[39] Y.H. Xu, C.J. Liu, M.J. Chen, Y.Q. Liu, A review in visible-light-driven $BiVO_4$ photocatalysts, International Journal of Nanoparticles 4 (2011) 268–283.
[40] A.P. Zhang, Z.J. Zhang, Hydrothermal processing for obtaining of $BiVO_4$ nanoparticles, Materials Letters 63 (2009) 1939–1942.
[41] G.P. Dai, S.Q. Liu, Y. Liang, T.X. Luo, Synthesis and enhanced photoelectrocatalytic activity of p–n junction Co_3O_4/TiO_2 nanotube arrays, Applied Surface Science 264 (2013) 157–161.
[42] W.Y. Su, J.X. Chen, L. Wu, X.C. Wang, X.X. Wang, X.Z. Fu, Visible light photocatalysis on praseodymium(III)-nitrate-modified TiO_2 prepared by an ultrasound method, Applied Catalysis B 77 (2008) 264–271.
[43] F. Duan, Y. Zheng, M.Q. Chen, Flowerlike $PtCl_4$/Bi_2WO_6 composite photocatalyst with enhanced visible-light-induced photocatalytic activity, Applied Surface Science 257 (2011) 1972–1978.